THERMODYNAMIC CHARACTERIZATION & SCALING OF A MEMS HEAT ENGINE

H. Bardaweel[1], R. Richards[1], M. Anderson[2], C. Richards[1]
[1]School of Mechanical and Material Engineering
Washington State University Pullman, WA, USA
[2]Dept. of Mechanical Engineering
University of Idaho, Moscow ID, USA

ABSTRACT: The working cycle of a MEMS dynamic heat engine has been acquired experimentally. The cycle approximates a vapor Carnot cycle and has a second law efficiency of 16%. A scaling analysis based upon a lumped parameter dynamic model was performed. The scaling analysis indicates that larger engines and different working fluids can lead to significantly higher efficiencies.

Keywords: Dynamic MEMS Heat Engine, Resonant Engine

INTRODUCTION

Although waste heat recovery has been successful in large scale power sources it is seldom done in small scale applications. For small scale power sources such as automobiles, home heating furnaces, and building HVAC systems there is no commercially viable approach to recover and utilize the waste heat. Although considerable effort has been directed to developing thermoelectric harvestors [1, 2], to date this approach, while making significant advances has not yet led to cost effective solutions to harvesting waste heat on the small scale. This is because the economics of waste heat harvesting is driven by the capital cost of the harvester.

Our group has worked to develop a microscale dynamic heat engine for waste heat harvesting. The design is based on simple 2D structures that are amenable to batch manufacturing with inexpensive materials. This design strategy has evolved from prior work aimed at developing a MEMS heat engine using combustion of fuel as a heat source to produce power for military applications. In these applications, engine size, along with energy density and power density are the driving metrics. Engine cost is of secondary concern. Much of the previous effort was focused on developing each of the components and then integrating them into a system. The results of that effort appear in the archival literature [3, 4].

The engine, which has no macroscale counterpart, is relatively unique compared to other micro engines [5]. In the design of the engine, we have exploited the dominance of surface tension at small scales to enable the compression and expansion of a two-phase fluid – a practical impossibility at the macroscale. Thus for the first time in any practical engine design, the implementation of a vapor Carnot cycle becomes a realistic possibility. A single flexible membrane acts as both compressor and expander [3]. We have shown that the engine is capable of producing net work, albeit at low efficiency. Now we turn to the application of waste heat harvesting and use a scaling analysis to explore designs that produce higher efficiencies that are economically viable for waste heat harvesting.

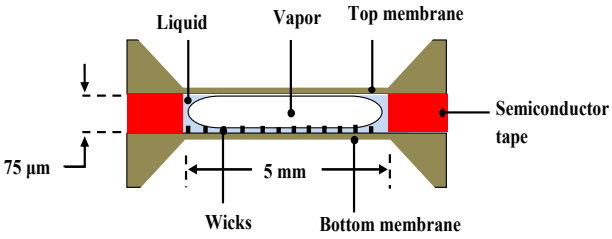

Fig. 1 Schematic of engine.

THEORY & EXPERIMENT

The micro engine, shown in Fig. 1, consists of a cavity filled with a two-phase fluid bounded by top and bottom membranes. The flexible top membrane acts as an expander. Mechanical power is produced as the top membrane alternately expands and compresses the working fluid. The rigid bottom membrane acts as an evaporator. A capillary wick fabricated on the bottom membrane controls the layer of liquid-phase working fluid on the evaporator. A thermal switch (not shown) is used to control the timing and duration of the heat addition and heat rejection. Details on the fabrication, assembly, and operation are provided in [3, 4].

The deflections of both the top and bottom membranes are measured with a laser vibrometer for a

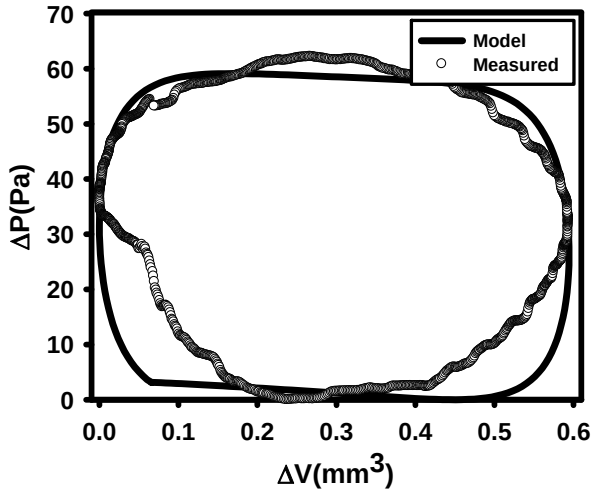

Fig. 2. P-V diagram of resonant operation.

given periodic heat input. Engine volume is derived from the top membrane deflection, and engine pressure is derived from the bottom membrane deflection. Pressure volume diagrams are constructed to characterize the working cycle of the engine.

The PV diagram for an engine operating at the resonance frequency is shown in Fig. 2. The experimental data are shown as symbols. The modeled data were obtained using a lumped parameter model. The cycle consists of two isobaric processes and two isochoric processes as shown in the figure. The processes take place under the saturation dome of the working fluid. This cycle approximates a vapor Carnot cycle. There are however, irreversibilities**.**

Although the engine cycle approximates a vapor Carnot cycle, the first law efficiency of the engine is very low. This is in part because the engine is operating over a very small temperature difference, only a few degrees at most. Using the pressure volume data, the temperature of the vapor at each point in the cycle was calculated. The second law efficiency was then calculated by comparing the work done by the engine to that which would be done by a Carnot engine operating across the same temperature difference. The second law efficiency of this engine is 16%, modest but promising.

In previous work we have developed and validated a lumped parameter model which captures the basic physics associated with both the thermal and dynamic processes in the engine [4]. A linearized version model takes the form

$$\Delta\dot{V}+\left[\frac{(\pi r_i^2)^2}{s_h}+\frac{V_o}{\rho_o R T_o}\right]\Delta\dot{p}-\frac{V_o}{T_o}\Delta\dot{T}=\frac{BS}{\rho_o}\Delta T_l -\frac{S}{\rho_o}\sqrt{\frac{M}{2\pi R_u}}\frac{1}{\sqrt{T_o}}\left[\Delta p-\frac{\rho_o R}{2}\Delta T\right], \tag{1}$$

$$\frac{V_o}{T_o}\Delta\dot{T}-\frac{V_o}{\rho_o c_p T_o}\Delta\dot{p}=-\frac{h_B}{\rho_o c_p T_o}\Delta T\,, \tag{2}$$

$$\frac{m+\overline{m}}{\left(\pi r_o^2\right)^2}\Delta\ddot{V}+\frac{b_f+b}{\left(\pi r_o^2\right)^2}\Delta\dot{V}+\frac{s}{\left(\pi r_o^2\right)^2}\Delta V=\Delta p\,, \tag{3}$$

$$\frac{C_T}{\rho_o h_{fg}}\Delta\dot{T}_l=\frac{q(t)}{\rho_o h_{fg}}-\frac{U}{\rho_o h_{fg}}\Delta T_l-\frac{B}{\rho_o}\Delta T_l +\frac{S}{\rho_o}\sqrt{\frac{M}{2\pi R_u}}\frac{1}{\sqrt{T_o}}\left[\Delta p-\frac{\rho_o R}{2}\Delta T\right], \tag{4}$$

where ΔV is the volume change of the vapor bubble caused by motion of the upper membrane; Δp, ΔT, and ΔT_l are the departures of vapor pressure, temperature, and liquid temperature from their ambient values. The coefficients represent thermal and mechanical properties of the working fluid and mechanical structure respectively, details can be found in [4].

Now we apply the scalings

$$\Delta V^*=\frac{\Delta V}{V_o},\ \Delta P^*=\frac{\Delta P}{P_o},\ \Delta T_l^*=\frac{\Delta T_l}{T_o},\quad q^*=\frac{q}{\omega\rho_o h_{fg}V_o},\ t^*=\omega t, \tag{5a-e}$$

for the dependent variables and time to the lumped parameter model (1-4), also neglecting evaporator flexibility and parasitic heat losses from the vapor bubble. In these scalings, the frequency ω is a reference mechanical frequency $\omega=\sqrt{m/s}$. The system model in non-dimensional form becomes

$$\frac{d^2\Delta V^*}{dt^{*2}}+\frac{1}{Q}\frac{d\Delta V^*}{dt^*}+\Delta V^*=F\Phi\Delta P^*,$$
$$\frac{d\Delta V^*}{dt^*}+\frac{d\Delta P^*}{dt^*}=-N\Phi\frac{\gamma+1}{2\gamma}\Delta P^*+N\Phi(BT_o)\Delta T_l^*, \tag{6-8}$$
$$C\frac{d\Delta T_l^*}{dt^*}=N\Phi\frac{\gamma+1}{2\gamma}\Delta P^*-\left[\overline{U}+(BT_o)N\Phi\right]\Delta T_l^*,$$

where

$$Q=\frac{m\omega}{b+b_f},\quad F=\frac{\pi r_o^2 P_o}{m\omega},\quad N=\frac{1}{\rho_o}\sqrt{\frac{M}{2\pi R_u}}\frac{P_o}{\sqrt{T_o}}, \tag{9a-f}$$
$$\Phi=\frac{S}{\omega V_o},\quad C=C_T\frac{T_o}{\rho_o h_{fg}V_o},\quad \overline{U}=\frac{U}{\omega}\frac{T_o}{\rho_o h_{fg}V_o}.$$

Several nondimensional numbers Q, C, $\overline{U}$ and products $F\Phi$ and $N\Phi$ are identified. The quantities C and $\overline{U}$ account for thermal inertia and parasitic conductive heat losses. The dimensional quantities F, N, and Φ account for mechanical properties associated

with engine flexing, thermal properties of the working fluid, and time-geometry properties of the engine respectively.

DISCUSSION

We hypothesize that the thermal inertia C, time-geometry factor Φ, and working fluid evaporation property N are the parameters that dominate the performance of a flexing resonant heat engine.

For example, suppose the working fluid N is fixed, and the thermal inertia C and time-geometry factor Φ are allowed to vary one order of magnitude higher and lower than those encountered in the MEMS-scale engine considered in [4], here denoted as C_o and Φ_o. As C and Φ are varied, the first-law efficiency of a flexing engine is computed.

A surface plot of the first-law efficiency for variations in the thermal inertia and time geometry factor is shown in Fig. 3. Consistent with prior conclusions [4], first law efficiency is highly sensitive to thermal inertia. For example, at the nominal time-geometry of $\Phi/\Phi o=1$, as thermal inertia is reduced to $C/C_o=0.1$, the first law efficiency improves from 1.1% to 19%. However, an improvement can also be obtained by varying the time-geometry factor. At the nominal thermal inertia $C/C_o=1$, as the time-geometry factor Φ is raised to $\Phi/\Phi_o=10$, the efficiency improves from 1.1% to 4.7%. When thermal inertia is reduced while simultaneously time-geometry is increased by one order of magnitude, a first-law efficiency of 50.2% is computed.

The composition of the non-dimensional thermal inertia C and the time-geometry factor imply that larger engines should perform at higher first-law efficiency. In the non-dimensional thermal inertia C, the dimensional lumped thermal inertia parameter C_T is scaled against the engine vapor volume V_o, and the latent evaporation property $\rho_o h_{fg}$ of the working fluid. Consequently, it is reasonable to expect that the non-dimensional thermal inertia C will decrease for larger engines and for working fluids with high latent evaporation.

The time-geometry factor Φ is composed of the reference frequency ω, and the ratio of evaporation-area S to engine volume V_o. It is also reasonable to expect that the reference frequency $\omega = \sqrt{m/s}$ for a large engine is lower than that for a small engine because it is easier to incorporate compliant geometry and more mass in a larger engine. In this case, the time-geometry factor Φ will be increased.

A second benefit predicted by the preliminary analysis is that a larger engine will be less affected by parasitic mechanical damping. In the computation of

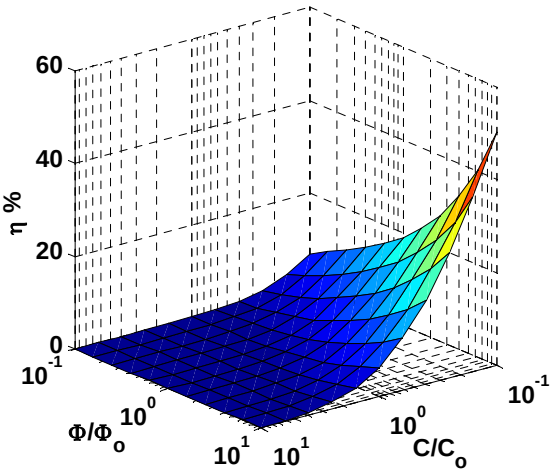

Fig. 3. First-law efficiency versus thermal inertia and time-geometry factor.

first-law efficiency, it is assumed without loss in generality that parasitic mechanical damping b_f is $b_f=0$. As found previously [4], optimal first-law efficiency for a given resonant flexing engine is obtained when the energy conversion device, modeled by the damping coefficient b, is load-matched to the engine. Consequently, for each flexing engine, there is an optimal mechanical quality factor Q_{opt}. In the preliminary analysis, as the thermal inertia C and time-geometry factor Φ are varied, the optimal quality factor Q_{opt} is also recorded. A surface-plot of the optimal quality factor Q_{opt} is shown in Fig. 4. At the nominal condition, $C/C_o=1$ and $\Phi/\Phi_o=1$, the optimal quality factor Q_{opt} is computed to be $Q_{opt}=61.9$. If, in the actual engine, parasitic mechanical damping was indeed negligible, it would be necessary to design an energy conversion device that resulted in a

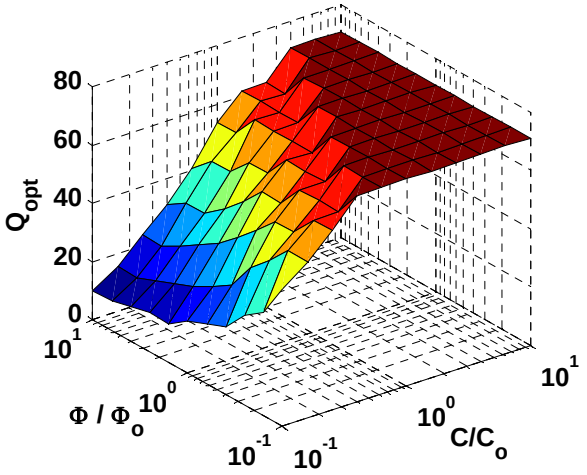

Fig. 4. Optimal quality factor versus thermal inertia and time-geometry factor.

mechanical quality factor of Q_{opt}=61.9. This is quite a large quality factor. In actuality, a smaller quality factor was observed in experiment with the MEMS-scale engine (Q ranged from 8 to 26), caused only by parasitic mechanical damping. However, the preliminary analysis shows that the optimal quality factor Q_{opt} is also sensitive to the thermal inertia C and time-geometry factor Φ. In fact, the optimal quality factor Q_{opt} declines significantly as thermal storage C and time-geometry factor Φ are decreased and increased respectively. For example, at a thermal inertia of C/C_o=0.1 and time-geometry factor of Φ/Φ_o=10, the optimal quality factor reduces to a value of Q_{opt}=10.27, a significant reduction from Q_{opt}=61.9 at the nominal condition. This reduction is fortuitous. Since the mechanical quality factor for an actual engine will be controlled by the sum of energy conversion and parasitic damping, $b+b_f$, a smaller optimal quality factor Q_{opt} relaxes the constraint on the amount of parasitic damping that may be tolerated. The thermal inertia C/C_o=0.1 and time-geometry Φ/Φ_o=10 are precisely those that would be expected for a larger engine. It is reasonable to expect that parasitic mechanical damping is easier to control for larger engines, given that viscous penetration depths are small fractions of overall dimensions.

This scaling analysis indicates that there are engine designs that can deliver relatively high efficiencies so that they are likely to be competitive for waste energy harvesting. Experimental realization of large variations in the thermal inertia term, C, may be realized by using different working fluids. For example, FC77, the fluorinert used in previous experiments, has a latent heat of vaporization equal to 89 kJ/kg. An alcohol such as ethanol, has a latent heat of vaporization of 855 kJ/kg. Water has a latent heat of vaporization of 2,260 kJ/kg. Thus by using different working fluids we can make order of magnitude changes in the thermal inertia term.

The time geometry factor Φ may be varied through changes in engine geometry. The analysis shows that we wish to increase this factor. Since we know that increasing S/V_o will be unfavorable for heat transfer, we can keep S/V_o constant or even decrease it. The engine cavity is essentially a box with a surface area equal to that of the membrane with sidelength a; that is, the surface area is a^2. The volume is then a^2h (h is the cavity height). And so the surface to volume ratio is equivalent to $1/h$. Thus we may scale up the engine and keep S/V_o constant by increasing the side length of the membrane and maintaining the thickness of the engine cavity. As the engine size increases the resonance frequency scales as $1/a^2$ (similar to a plate in flexure). Increasing the side length of the membrane by a factor of 3 will lead to almost an order of magnitude decrease in the resonance frequency and thus an order of magnitude increase in the time geometry factor.

Ultimately the goal is to evolve designs that use inexpensive materials and manufacturing processes. Thus, although the use of silicon and associated machining techniques is convenient for laboratory studies, it is not likely to be an economical design. In fact, it is likely that the scaling study will lead to designs that become difficult to realize in silicon; i.e., thin membranes with large surface area. The engine is designed to be amenable to manufacture by the stacking of thin films or laminates. Many polymers are less expensive than single crystal silicon, and in addition, offer the use of cheaper manufacturing techniques such as, molding, spin casting, and spraying. Candidate polymers include polyimides, PMMA, PDMS, and fluorocarbon films.

CONCLUSIONS

The working cycle of a MEMS dynamic heat engine has been acquired experimentally. The cycle approximates a vapor Carnot cycle and has a second law efficiency of 16%. A scaling analysis was performed to identify designs that lead to higher efficiencies. The analysis indicates that larger and more compliant engines along with alternative working fluids can lead to significantly higher first law efficiencies.

REFERENCES

[1] Venkatasubramanian R, Watkins C, Caylor C, Bulman G 2006 Microscale thermoelectric devices for energy harvesting and thermal management *Technical Digest PowerMEMS 2006 (Berkeley, CA, 28–29 November 2006)*

[2] Venkatasubramanian, E. Siivola, T. Colpits, B. O'Quin, Nature, Vol. 413, 597 – 602, 2001.

[3] Bardaweel HK, Anderson MJ, Richards RF, Richards CD 2008 Optimization of dynamic and thermal performance of a resonant micro heat engine *J. Micromech. Microeng.* **18** 104014

[4] Cho J, Weiss L, Richards C, Bahr D and Richards R 2007 Power production by a dynamic heat engine with an integrated thermal switch *J. Micromech. Microeng.* **17** S217–S223

[5] Jacobson SA & Epstein AH 2003 An informal survey of power MEMS *International Symposium Micro-Mechanical Engineering ISMME (Japan, Dec 1 -3 2003)*